Subcellular targeted anionophores

William G. Ryder,[a,c] Marcus E. Graziotto,[a] Elizabeth J. New,[a,b] and Philip A. Gale.*[a,c]

[a] School of Chemistry, The University of Sydney, Sydney, NSW, 2006, Australia.

[b] Australian Research Council Centre of Excellence for Innovations in Peptide and Protein Science, The University of Sydney, Sydney, NSW, 2006, Australia.

[c] School of Mathematical and Physical Sciences, Faculty of Science, University of Technology Sydney, Ultimo, NSW 2007, Australia.

philip.gale@uts.edu.au

Abstract

Synthetic anion transporters that mediate electroneutral (H^+/Cl^-) transport have demonstrated anti-cancer activity due to their ability to disrupt subcellular homeostasis. Elucidation of the cell death mechanism revealed the transporters' ability to neutralise lysosomal pH gradients and inhibit autophagy. However, their effect on other subcellular compartments is unknown. Herein, we disclose the first subcellular targeted anionophores that accumulate in various membrane bound organelles to bias their natural propensity to depolarise lysosomes. The series of naphthalimide-based transporters were studied by confocal microscopy, and were found to accumulate in different subcellular organelles. The analogues that contained endoplasmic reticulum (ER)- and lysosomal targeting motifs showed enhanced the H^+/Cl^- transport ability compared to their non-targeted analogues. Moreover, ER and lysosomal localisation was found to enhance the cytotoxic effect of the transporters on cancerous cells. Our work provides an alternative approach in the design of therapeutically focused synthetic anion transporters and an insight into possible subcellular compartment-specific effects on homeostasis.

Introduction

The precise regulation of anionic species across phospholipid bilayers is fundamental to pH regulation, cellular signalling, osmotic balance, and many other biological processes crucial for cellular function.[1-3] Synthetic molecules capable of facilitating anion transmembrane transport have attracted significant interest as potential therapeutics in the treatment of diseases associated with ion transport dysregulation,[4] such as cystic fibrosis,[5] or as novel anti-cancer agents.[6] Recently, synthetic anion transporters have been shown to match and even surpass the transport abilities of biological chloride channels and natural products.[7,8] As a result, there is a growing focus towards evaluating their cellular effects.[9] It has been shown that electroneutral (H^+/Cl^-) anionophores induce apoptosis by decreasing the lysosomal chloride concentration, which leads to an increase in lysosomal pH and disruption of lysosomal function essential for autophagy.[10-11]

Mammalian cells are incredibly complex and possesses many compartmentalised membrane-bound organelles, each with a specific structure and function vital for cellular function. Common examples include mitochondria, which form the foundation of energy production from oxidative phosphorylation.[12] The endoplasmic reticulum (ER) is involved in synthesising lipids and proteins that are subsequently sorted and modified through post-translational modifications in the Golgi apparatus,[13-14] and lysosomes are responsible for cellular digestion essential to autophagy.[15] While the determinants of cancer cell death exhibited by the previously-tested anionophores were found to exert their effects on the lysosomes,[10] the effect of anionophore-induced transport on other subcellular

compartments is currently unknown. Concomitant chloride transport proteins have been identified in other subcellular compartments such as the ER, Golgi apparatus and mitochondria, which highlights the importance of this anion to the cellular function of many membrane-bound organelles.[16-19] We hypothesised that anionophores which can selectively target unexplored membrane-bound organelles might elicit different physiological responses.

Herein, we demonstrate this concept by developing a series of fluorescent anionophores, compounds **1**–**9**, that have been designed to localise in different subcellular compartments. The appendage of organelle-targeting motifs maintained, and in some cases increased, the anion binding and transport ability of the receptors, while live cell confocal laser scanning microscopy confirmed their organelle-specific localisation. All the anionophores demonstrated cytotoxicity towards cancer cells. Notably, transporters that demonstrated lysosomal or ER localisation were found to enhance the cytotoxicity compared to non-targeted transporters, representing an alternative approach in the development of antineoplastic-oriented synthetic anionophores.

Synthesis and characterisation.

Compounds **1**–**9** were constructed around a fluorescent 1,8-naphthalimide core. The scaffold has been used extensively in sensing and cellular imaging due to its desirable photophysical properties.[20-21] Urea-based receptors have found numerous applications in the field anion recognition due to their widely recognised binding properties and were chosen as the binding motif for compounds **1**–**9**.[22] Moreover, we have previously demonstrated the anionophoric ability and cytotoxicity of compound **9**, which was found to disperse homogenously in the cytosol.[23] The 1,8-anhydride derivative of this scaffold allows for a high degree of functionalisation which we chose to exploit through the appendage of subcellular targeting motifs. Additionally, the distal nature of the anhydride minimised possible sterically encumbering interactions between the targeting groups with the hydrogen bonding cavity. There are several strategies for achieving sub-cellular targeting, including targeting peptides and self-labelling peptides. We opted to use well-established small molecule targeting groups, to ensure effective transmembrane transport.[24] We opted to incorporate simple lipophilic groups, which align well with the properties required for effective transmembrane transport. To target the lysosomes, we incorporated morpholino- and *N,N*-dimethylethyl motifs due to their reversible protonation at physiological pH.[25] Cyclohexylsulfonyl urea and *p*-toluenesulfonamide motifs were used for targeting the ER.[26-28] We utilised triphenyl phosphoniums to specifically target the mitochondria, as these moieties are renowned for their propensity to accumulate within the negatively charged inner mitochondrial membrane facilitated by the transmembrane proton pump.[29-30] A non-targeting hydrophilic polyethylene glycol chain, compound **8**, was synthesized alongside the previously-studied compound **9** to probe the activity of the transporters in the absence of targeting groups.[23] Lastly, a non-targeted control bearing a secondary amine, compound **10**, was synthesised to evaluate the importance of the hydrogen bonding urea motif.

The synthesis of each anionophore **1**–**9** was achieved in 4-8 steps, each initiated by the construction of their respective targeting motif. The appropriate ethyl- and propylamine precursors were then incorporated into the central scaffold in good to excellent yields through a condensation reaction with 4-bromo-1,8-naphthalimide. Subsequent azide substitution and reduction afforded the 4-amino intermediates, which were transformed into their respective isocyanates using triphosgene. The addition of 3,5-bistrifluoromethyl aniline afforded compounds **1**–**9** in low to excellent yields. Compound **10** was ultimately synthesised from the condensation of pentylamine with 4-bromo-1,8-

naphthalimide, followed by a substitution with a second equivalent of pentylamine which afforded **10** in excellent and moderate yields, respectively.

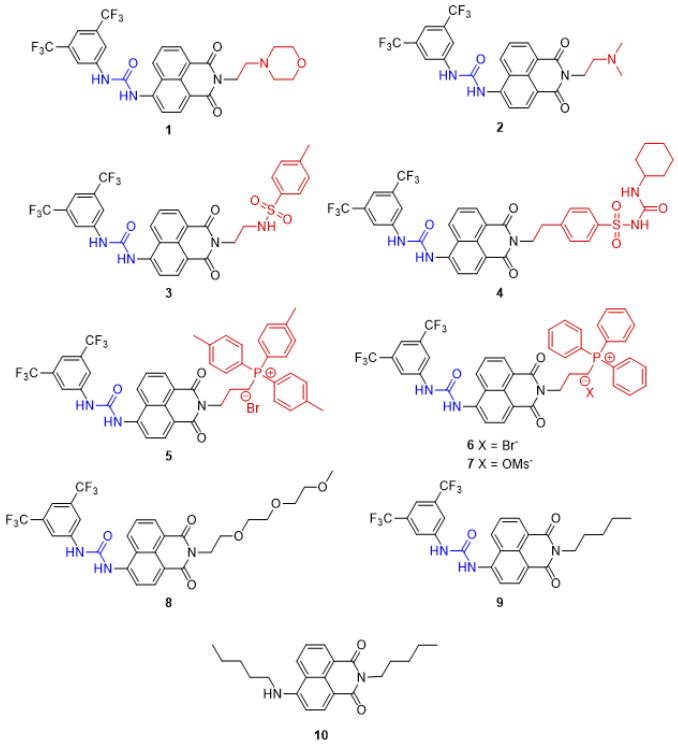

Figure 1. Structures of the fluorescent anion transporters studied in this paper. Subcellular targeting anionophores **1**–**7**, non-targeting anionophores **8** and **9**, and control naphthalimide **10**. Blue = anion binding motif. Red = subcellular targeting group.

Anion binding in solution

The binding affinities of compounds **1**–**10** were assessed using ^{1}H NMR titrations in DMSO-d_6/0.5% water. Solutions of each receptor were titrated with up to 200 equiv. of tetrabutylammonium chloride (TBACl). Large downfield shifts from both the urea protons and smaller shifts from the aromatic naphthalimide CH were observed upon the addition of TBACl for receptors **1**–**9**, while a separate downfield shift of the amine proton was exhibited by compound **10**.

Table 1. Summary of chloride binding properties of receptors **1**–**10**.

Compound	K_a Cl^- [a]
1	163
2	171
3	191
4	*K_{11}: 260; K_{12}: 7
5	156
6	269
7	299
8	165
9	177
10	2

[a] Association constant (M^{-1}) calculated by fitting the change in chemical shifts upon addition of tetrabutylammonium chloride (TBACl) of the urea NH and the naphthalimide CH resonance to a 1 : 1 binding model. *Calculated by fitting the change in chemical shifts upon addition of TBACl of the urea NH, naphthalimide CH and sulfonyl urea NH resonances to a 1 : 2 binding model.

All receptors were fit to both 1 : 1 and 1 : 2 receptor:guest binding models using a global fitting applet to generate the association constants shown in **Table 1**. [31-32] Receptor **4** possesses a sulfonyl urea on appended targeting moiety, which has previously been used in the construction of anion receptors.[33] In the presence of chloride, downfield shifts were observed by both sulfonyl urea protons of **4** and, accordingly, was the only receptor to exhibit a good fit to a 1 : 2 binding model whereas the remaining receptors displayed a better fit to a 1:1 binding model. Compounds **1**–**9** demonstrated moderate binding to chloride, while control receptor **10** showed almost no complexation to chloride, highlighting the importance of the dual hydrogen bonding motif for successful anion binding. The strongest affinity was observed for receptors **6** and **7**, presumably due to additional electrostatic interactions from the charged targeting groups stabilising the host-guest complex. Strikingly, the similarly charged receptor **5** showed the weakest complexation to chloride. While we anticipated a modest decrease in the positively charged character of the phosphonium ion in compound **5**, attributed to the positive inductive effects of the methylated aryl rings, the magnitude of this effect in the calculated association constants exceeded our expectations. The highest affinity across the neutral receptors was exhibited by receptor **3**. The single sulfonamide is likely too weak to create its own separate binding cavity but was found to enhance the overall affinity to chloride. Despite the addition of different targeting motifs, the binding affinities to chloride remained broadly similar across the neutral receptors, which justified our decision to position the targeting motifs further away from the anion-binding motif.

Transport studies

Motivated by the binding capabilities of **1**–**9**, the anionophoric ability of the naphthalimides was demonstrated using the Cl^-/NO_3^- exchange assay. Palmitoyl-2-oleoyl-*sn*-glycero-3-phosphocholine (POPC) large unilamellar vesicles (LUVS, 200 nm) were entrapped with NaCl (489 mM, buffered to pH 7.2 using phosphate salts) and suspended in an external solution of $NaNO_3$ (buffered under the same conditions). Transporters were added as a DMSO solution (10 µL) at *t* = 0 s to initiate anion exchange across the membrane, and the increase in extravesicular chloride concentration was measured using an ion-selective electrode (ISE). The vesicles were treated with Triton X-100 at *t* = 300 s to lyse the contents into the external solution and calibrate the 100% chloride efflux value. **Figure 2.** shows the results of Cl^-/NO_3^- exchange experiments at 1 mol% loading of each anionophore (with respect to lipid concentration).

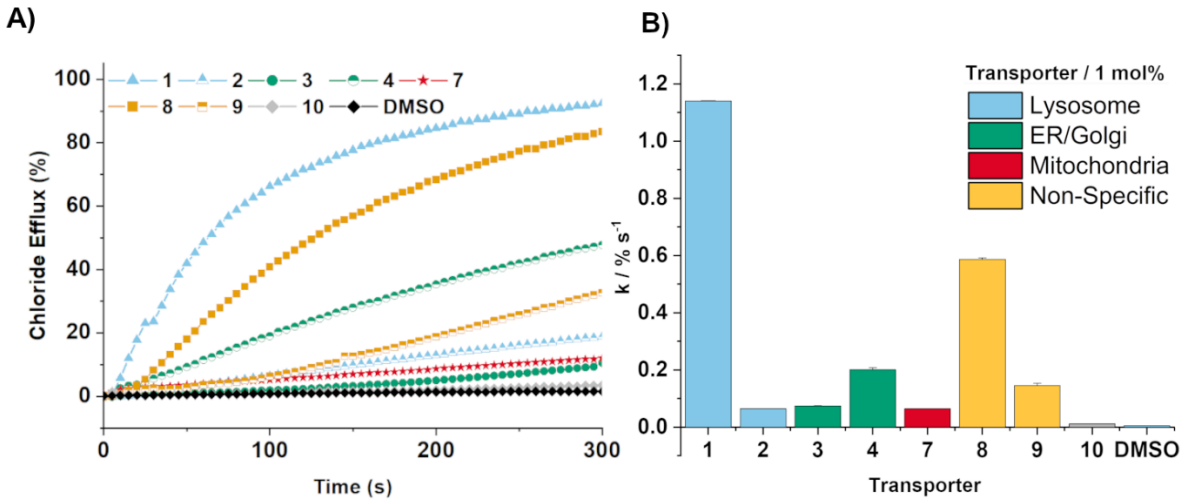

Figure 2. A) Chloride efflux as a function of time promoted by the addition of 1 mol% (with respect to lipid concentration) of anionophores **1**–**4** and **7**–**10** using POPC LUVs entrapped with 489 mM NaCl buffered to pH 7.2 with 5 mM sodium phosphate salts suspended in 489 mM $NaNO_3$ buffered to pH 7.2 with 5 mM sodium phosphate salts. The receptors were added as a DMSO solution. At *t* = 300 s (the end point of the experiment), the vesicles were lysed with Triton X-100 to calibrate the 100% chloride efflux. Each point is an average of three repeated runs. **B)** Calculated initial rates from the chloride efflux as a function of time promoted by the addition of 1 mol% (with respect to lipid concentration) of anionophores **1**–**4** and **7**–**10**.

In comparison to the simple pentyl analogue **9**, the anionophores were all found to effectively transport chloride, despite the added complexity of the affixed targeting moieties. It should be noted that the addition of compound **6** to the Cl^-/NO_3^- exchange assay led to a spike in the initial transport rate, presumably due to interference from the bromide counter anion, and therefore was omitted from the assay. Additionally, the assessment of the anion transport ability of **5** could not be completed due to the insolubility of the receptor. Morpholine-appended compound **1** displayed the highest potency across the series and was significantly more active than the other lysosomal-targeting analogue compound **2**. Amongst the proposed ER targeting receptors, higher activity was exhibited by **4** compared to **3,** which could be rationalised by the presence of the additional anion binding motif within compound **4**. Membrane permeability is heavily inhibited by charged species and could be a possible reason for the lower transport activity demonstrated by the triphenyl phosphonium-containing compound **7**. Both compounds that lacked targeting groups, **8** and **9,** were shown to efficiently mediate Cl^-/NO_3^- exchange. Remarkably, the addition of the polyethylene glycol chain to compound **8** resulted in a four-fold increase in the Cl^-/NO_3^- exchange rate compared to the highly lipophilic pentyl analogue **9** (**Table 1.**). To the best of our knowledge, this is the most active anionophore bearing this highly hydrophilic group. This modification has the potential to enhance the intrinsic deliverability of anionophores in aqueous solutions while retaining potent activity, an active area of transmembrane transport we are persistently looking to explore.[34-35]

Overall, the transport activity was found to contest the trends uncovered in the solution-phase binding studies. This is a consequence of the targeting groups influencing the ability of each anionophore to partition through the membrane. Lipophilicity determines the ability of a transporter to partition through the lipid bilayer and has been demonstrated to be an important consideration when determining transmembrane transport activity. While no obvious correlation was elucidated with

respect to lipophilicity, we found that the structurally simple targeting groups displayed the highest rate of Cl^-/NO_3^- exchange. From this, we theorised that the diminished activity observed could result from possible adverse interactions with the phospholipid lipid bilayer from transporters that possess an inherent charge or additional hydrogen bond donors.

We then sought to determine the mechanism of chloride transport mediated by the anionophores using a cationophore-coupled assay using natural ionophores, valinomycin and monensin. POPC LUVs loaded with KCl (300 mM, buffered to pH 7.2 using phosphate salts) were suspended in potassium gluconate (KGlu, 300 mM, buffered to pH 7.2 using similar conditions). Transporters were added as a DMSO solution (10 µL) at *t* = 0 s to initiate efflux, and the increase in chloride concentrations in the external solution was measured using an ISE. The vesicles were treated with Triton X-100 at *t* = 300 s to lyse all contents into the external solution and calibrate the 100% chloride efflux value.

Electrogenic transport implies the transmembrane uniport of chloride, which generates a membrane potential that can be balanced through an independent electrogenic transport event (for example, the transport of a cation or back exchange of another anion). In contrast, electroneutral transport does not lead to a net transfer of charge. Instead, it involves the simultaneous transport of two ions (one anion and one cation, or two different anions) in a process which cannot be separated. The external solution utilises the highly hydrophilic and membrane-impermeable gluconate; thus, the addition of the anionophore alone will not initiate transport as there is no counterflow of anions to alleviate the build-up of negative charge. Valinomycin strictly mediates the uniport of K^+ across the phospholipid bilayer and, consequently, coupling to valinomycin signifies the electrogenic uniport of Cl^- facilitated by the anionophore. In contrast, monensin exchanges H^+/K^+ across the lipid membrane and coupling of an anionophore to monensin implies an electroneutral H^+/Cl^+ symport mechanism mediated by the transporter. We concluded that anionophores **1**-**4** and **7**-**9** were capable of both electrogenic and electroneutral Cl^- transport, with a modest selectivity for H^+/Cl^- transport across all the tested anionophores. Implementing different targeting motifs offered no change in the transport mechanism, even in the presence of additional binding components, in the form of sulfonyl ureas, or electrostatic charges.

The transport activity was further evaluated through a fluorescence-based assay. POPC LUVs were loaded with the pH-responsive fluorophore 8-hydroxypyrene-1,3,6-trisulfonate (HPTS) and N-methyl-D-glucamine (NMDG) chloride, buffered to pH 7.0 with HEPES. The vesicular solution was suspended in an external aqueous solution of NMDG-Cl, similarly, buffered to pH 7.0 with HEPES. A pH gradient was applied across the membrane through the addition of an NMDG base pulse, followed by the addition of the transporter as a DMSO solution (10 µL) to initiate transport. The ability of a transporter to dissipate the pH gradient through H^+/Cl^+ symport (or equivalent OH^-/Cl^- antiport) was determined through the change in the fluorescence emission spectra of HPTS. At the end of the run, the vesicles were similarly treated with Triton X-100 to calibrate the 100% chloride efflux value.

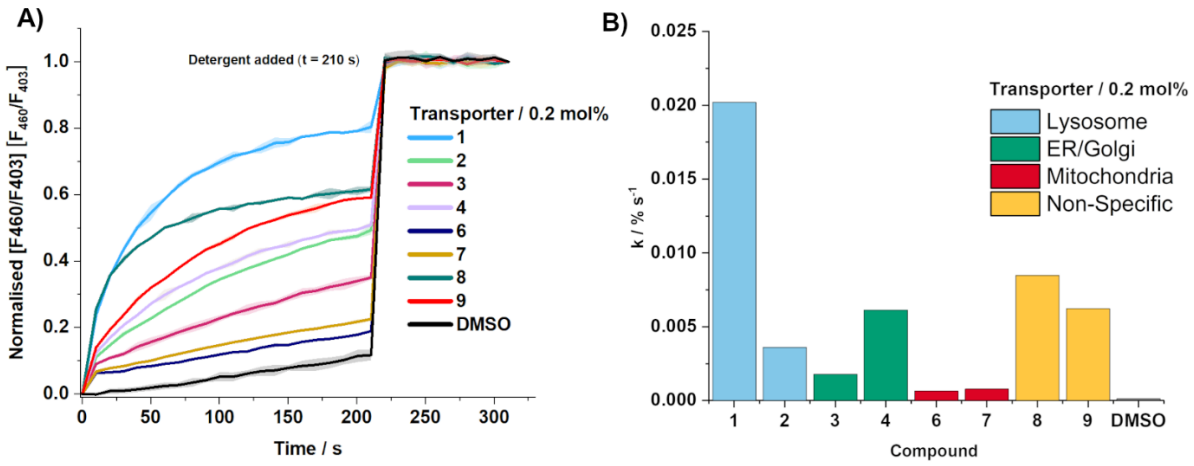

Figure 3. A) Chloride efflux as a function of time promoted by the addition of 0.2 mol% (with respect to lipid concentration) of anionophores **1**–**4** and **6**–**9** using POPC LUVs entrapped with NMDG-Cl buffered to pH 7.0 with HEPES, suspended in NMDG-Cl buffered to pH 7.0 with HEPES. An NMDG base pulse generated a pH gradient and the receptors were added as a DMSO solution. At 210 s (the end point of the experiment), the vesicles were lysed with Triton X-100 to calibrate the 100% chloride efflux. Each point is an average of three repeated runs. **B)** Calculated initial rates from the chloride efflux as a function of time promoted by the addition of 0.2 mol% (with respect to lipid concentration) of anionophores **1**–**4** and **6**–**9**.

In contrast to the ISE-based assays, the higher sensitivity of the HPTS assay allowed for a more complete and in-depth comparison of activity trends at a more biologically relevant concentration. **Figure 3A.** shows the activity of compounds **1**–**4** and **6**–**9** (0.2 mol%, relative to lipid concentration). The trends in initial transport rates were shown to mirror those observed in the Cl^-/NO_3^- exchange assay. Notably, the assay allowed the comparison of the two mitochondrial targeting compounds **6** and **7**, whereby a marginal increase in the transport rate was observed upon the substitution of the bromide counter ion for mesylate. To further quantify the anionophoric ability, the same assay was used to determine the concentration-dependent transport activity of each receptor. Dose-response curves were fit to the Hill equation to derive the effective concentration of a transporter required to reach 50% efflux (EC_{50}). An activity sequence of **1** > **8** > **2** = **4** > **9** was established, highlighting the high potency of the morpholine-appended anionophore **1**, with an EC_{50} value of 0.06 mol% (**Table 2.**). Alkyl chains are commonly employed in transmembrane transport to enhance lipophilicity and thus, increase the membrane permeability of transporters.[36-37] A comparison of the EC_{50} values serendipitously revealed that the substitution of the pentyl chain with various subcellular targeting motifs increased the efficiency of chloride transport. The most significant example was found in comparison of compounds **1** and **9**, where a 4-fold decrease in the EC_{50} was observed. The Hill coefficient, n, also provides an insight into the stoichiometry of the transport process. The analysis revealed that the coefficients were close to n = 1 in all cases, indicating a 1 : 1 transporter-anion stoichiometry.

Table 2. EC_{50} values shown for the NMDG-Cl assay.

Compound	EC_{50} [a] (mol%)	*n*
1	0.06	1.1
2	0.14	0.8
4	0.14	0.72
8	0.09	1.1
9	0.23	1.3

[a] Effective concentration needed to obtain 50% chloride efflux (EC_{50}) at 210 s, values reported in transporter to lipid molar ratio (mol%).

***In vitro* studies**

After establishing the anionophoric activity of our compound series, attention turned to exploring the subcellular localisation of **1**–**10** in cultured cells. To confirm that the compounds were suitable for cellular imaging, the cell viability at concentrations of transporters intended for imaging studies was assessed using an alamarBlue assay in A549 human lung carcinoma cells. All transporters displayed negligible cytotoxicity to the living cells when dosed with 1.5 μM for 24 h, and initial confocal microscopic experiments demonstrated bright intracellular fluorescence at various concentrations.

All the subcellular-targeted anionophores were found to localise in their targeted sub-cellular compartment. The emission of transporter **1** is shown in **Figure 4A.**, where punctate structures around the nucleus indicative of lysosomal staining were observed. To confirm the accumulation of **1** within the desired organelle, colocalisation experiments were performed with LysoTracker Deep Red (LTDR) (**Figure 4A**). The results confirmed the effective lysosomal targeting ability of **1**, and a calculated Pearson's correlation coefficient (PCC) of 0.80 further quantified the localisation. Similar experiments with compound **2** also revealed excellent lysosomal localisation, with a calculated PCC value of 0.90. Similar co-staining experiments with ER Tracker Red (ERTR) determined that compounds **3** and **4** (**Figure 4B.**) localised within the ER, with calculated PCC values of 0.78 and 0.74. Fluorescence images containing transporters **6** and **7** showed web-like fluorescent structures that correlated to the mitochondria (**Figure 4C.**). The excellent mitochondrial targeting capabilities of compounds **6** and **7** were confirmed through their colocalisation with MitoTracker Deep Red (MTDR), which gave calculated PCC values of 0.91 and 0.92, respectively. Non-targeting compound **9** and control compound **10** were observed to localise homogenously throughout the cytoplasm, with no observable colocalisation with any organelle marker. We envisaged that incorporating a polyethylene glycol chain would promote cytosomal accumulation due to the high hydrophilicity of this motif. No lysosomal or mitochondrial accumulation was observed by transporter **8**, but interestingly, we found modest localisation to the ER (**Figure 4D**). While there is a tendency of lipophilic compounds to localise in the ER, the mechanistic reasoning is poorly understood compared to other organelles. Localisation to the ER by non-targeting probes, such as **8**, is believed to be a direct result of a molecule's optimum hydrophobicity towards the organelle,[38] and for this reason, there are only a few other instances of ethylene glycol-directed ER targeting probes.[39-40]

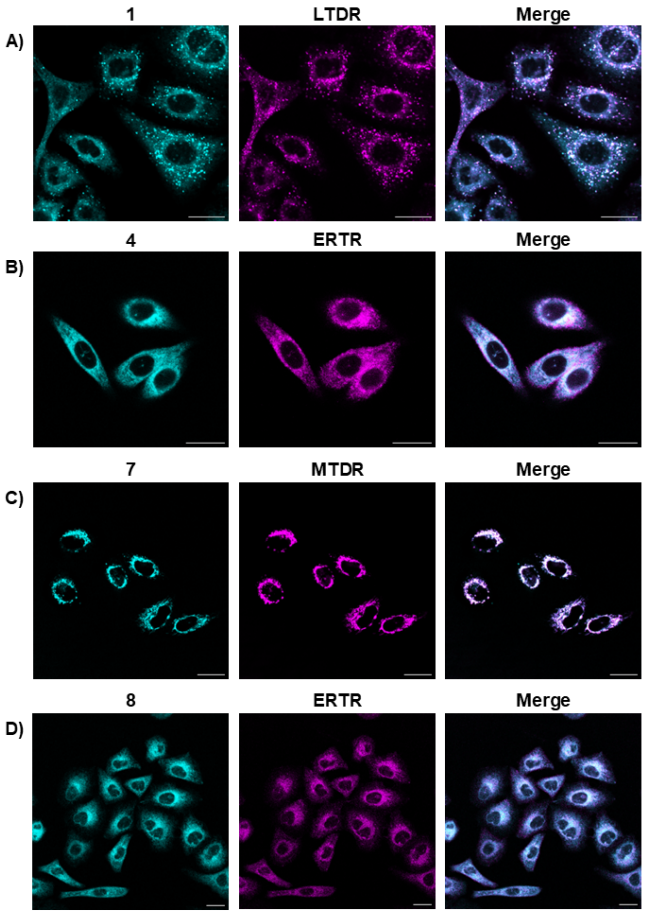

Figure: 4. Colocalisation experiments. Representative images of A549 cells dosed with: **A) 1** (1 µM) and LysoTracker Deep Red (LTDR) (50 nM) for 30 mins, **B) 4** (1 µM) and ER-Tracker Red (ERTR) (50 nM) for 30 mins; **C) 7** (1 µM) and MitoTracker Deep Red (MTDR) (50 nM) for 30 mins; **D) 8** (1 µM) and ER-Tracker Red (ERTR) (50 nM) for 30 mins. Cyan channel (transporter): λex = 287nm, λem = 482-582 nm. Magenta channel (LTDR, MTDR): λex = 640 nm, λem = 650–750 nm. Magenta channel (ERTR): λex = 561 nm, λem = 575–675 nm. Scale bars represent 20 µm.

We further investigated the cellular effects of compounds **1**–**4** and **6**–**10** by exploring their cytotoxicity in more detail using an alamarBlue™ assay. Through the calculated half maximum inhibitory concentration (IC_{50}) values, it was found that all urea-containing transporters effectively induced cell death, albeit to varying degrees. Compound **10**, on the other hand, was non-toxic, highlighting that the observed cytotoxicity in the cancer cell line is strongly correlated to the presence of the anion binding urea moiety. Remarkably, the extent of cytotoxicity from the lysosomal, ER, and mitochondrial targeting compounds was maintained despite their distribution to other subcellular components. Comparison of cell viabilities between mitochondrial transporters **6** and **7** showed no significant difference. Importantly, the more potent anionophores within the lysosomal and ER targeting groups demonstrated the highest cytotoxicity after 24 h. Lysosomal targeting anionophores **1** and **2** demonstrated the largest enhancement in cytotoxicity when compared to the non-targeting anionophore **9**. While the cell death mechanism of **9** is yet to be elucidated, it is possible that the lysosomal depolarisation pathway shown by other anionophoric scaffolds is responsible for the observed cytotoxicity. [10-11-41] We postulate that the increase in lysosomal accumulation demonstrated

by compounds **1** and **2** over **9** led to an increased perturbation of the lysosomal ionic and pH gradients, consequently enhancing the cytotoxicity. Compound **4** also exhibited a two-fold increase in cytotoxicity upon its subcellular accumulation to the ER compared to non-targeting anionophore **9**, we are currently investigating if these novel findings are initiated through new mechanisms of cell death outside the natural lysosomal pathway.

Compound	IC_{50} *(μM)*
1	4.4
2	5.3
3	35.1
4	6.6
6	11.4
7	11.9
8	>100
9	12.0
10	>200

Table 3. IC_{50} values of compounds **1**–**4** and **6**–**10** on the human lung carcinoma (A549) cell line after incubation for 24 h.

Conclusion

Based on the findings here, we present the first examples of subcellular targeted anionophores which accumulate in organelles previously unexplored in the context of anion transmembrane transport. The incorporation of organelle-specific motifs to a naphthalimide scaffold afforded a library of fluorescent receptors capable of anion binding and transmembrane transport at micromolar concentrations. By exploiting lipophilic subcellular targeting motifs, we enhanced the electroneutral chloride transport ability of the anionophores compared to their non-targeting analogues. Fluorescence microscopy in live cells confirmed the concentrated anionophoric accumulation in specefic membrane-bound organelles. We anticipate that the subcellular manipulation of anionophores will open up novel possibilities for initiating new subcellular compartment-specific effects on homeostasis, shaping the design in a new wave of therapeutically focused synthetic anion transporters.

References

1. F. M. Ashcroft, *Ion Channels and Disease*, Academic Press, San Diego, 2001.
2. N. B. EE Bittar, *Principles of medical biology*, JAI Press, 1997.
3. D. C. Gadsby, *Nat Rev Mol Cell Biol*, 2009, **10**, 344-352.
4. S. Hatta, J. Sakamoto and Y. Horio, *Med Electron Microsc*, 2002, **35**, 117-126.
5. H. Li, H. Valkenier, A. G. Thorne, C. M. Dias, J. A. Cooper, M. Kieffer, N. Busschaert, P. A. Gale, D. N. Sheppard and A. P. Davis, *Chem Sci*, 2019, **10**, 9663-9672.
6. S. Ohkuma, T. Sato, M. Okamoto, H. Matsuya, K. Arai, T. Kataoka, K. Nagai and H. H. Wasserman, *Biochem J*, 1998, **334**, 731-741.

7. H. Valkenier, L. W. Judd, H. Li, S. Hussain, D. N. Sheppard and A. P. Davis, *J Am Chem Soc*, 2014, **136**, 12507-12512.
8. X. Wu, J. R. Small, A. Cataldo, A. M. Withecombe, P. Turner and P. A. Gale, *Angew Chem Int Ed Engl*, 2019, **58**, 15142-15147.
9. J. T. Davis, P. A. Gale and R. Quesada, *Chem Soc Rev*, 2020, **49**, 6056-6086.
10. S. H. Park, S. H. Park, E. N. W. Howe, J. Y. Hyun, L. J. Chen, I. Hwang, G. Vargas-Zuniga, N. Busschaert, P. A. Gale, J. L. Sessler and I. Shin, *Chem*, 2019, **5**, 2079-2098.
11. N. Busschaert, S. H. Park, K. H. Baek, Y. P. Choi, J. Park, E. N. W. Howe, J. R. Hiscock, L. E. Karagiannidis, I. Marques, V. Felix, W. Namkung, J. L. Sessler, P. A. Gale and I. Shin, *Nat Chem*, 2017, **9**, 667-675.
12. L. Dard, W. Blanchard, C. Hubert, D. Lacombe and R. Rossignol, *Mol Aspects Med*, 2020, **71**, 100842.
13. D. S. Schwarz and M. D. Blower, *Cell Mol Life Sci*, 2016, **73**, 79-94.
14. K. J. Day, L. A. Staehelin and B. S. Glick, *Histochem Cell Biol*, 2013, **140**, 239-249.
15. F. R. M. J. M. Willard, and S. Lu, *Lysosomes : Biology, Diseases, and Therapeutics*, John Wiley & Sons, 2016.
16. B. O'Rourke, *Annu Rev Physiol*, 2007, **69**, 19-49.
17. R. R. Duncan, P. K. Westwood, A. Boyd and R. H. Ashley, *J Biol Chem*, 1997, **272**, 23880-23886.
18. Y. Maeda, T. Ide, M. Koike, Y. Uchiyama and T. Kinoshita, *Nat Cell Biol*, 2008, **10**, 1135-1145.
19. L. Guo, Q. Mao, J. He, X. Liu, X. Piao, L. Luo, X. Hao, H. Yu, Q. Song, B. Xiao, D. Fan, Z. Gao and Y. Jia, *Cell Res*, 2023, **0**, 1-19.
20. S. Banerjee, E. B. Veale, C. M. Phelan, S. A. Murphy, G. M. Tocci, L. J. Gillespie, D. O. Frimannsson, J. M. Kelly and T. Gunnlaugsson, *Chem Soc Rev*, 2013, **42**, 1601-1618.
21. C. Geraghty, C. Wynne and R. B. P. Elmes, *Coord Chem Rev*, 2021, **437**.
22. V. Amendola, L. Fabbrizzi and L. Mosca, *Chem Soc Rev*, 2010, **39**, 3889-3915.
23. S. N. Berry, V. Soto-Cerrato, E. N. W. Howe, H. J. Clarke, I. Mistry, A. Tavassoli, Y. T. Chang, R. Perez-Tomas and P. A. Gale, *Chem Sci*, 2016, **7**, 5069-5077.
24. J. Lin, K. Yang and E. J. New, *Org Biomol Chem*, 2021, **19**, 9339-9357.
25. T. M. P. Handbook, Life Technologies, 11 edn., 2010.
26. L. Fang, G. Trigiante, R. Crespo-Otero, C. S. Hawes, M. P. Philpott, C. R. Jones and M. Watkinson, *Chem Sci*, 2019, **10**, 10881-10887.
27. Y. Tang, A. Xu, Y. Ma, G. Xu, S. Gao and W. Lin, *Sci Rep*, 2017, **7**, 12944.
28. H. Xiao, C. Wu, P. Li, W. Gao, W. Zhang, W. Zhang, L. Tong and B. Tang, *Chem Sci*, 2017, **8**, 7025-7030.
29. M. P. Murphy and R. C. Hartley, *Nat Rev Drug Discov*, 2018, **17**, 865-886.
30. J. Zielonka, J. Joseph, A. Sikora, M. Hardy, O. Ouari, J. Vasquez-Vivar, G. Cheng, M. Lopez and B. Kalyanaraman, *Chem Rev*, 2017, **117**, 10043-10120.
31. app.supramolecular.org).
32. D. Brynn Hibbert and P. Thordarson, *Chem Comm*, 2016, **52**, 12792-12805.
33. D. Barisic, N. Cindro, N. Vidovic, N. Bregovic and V. Tomisic, *RSC Adv*, 2021, **11**, 23992-24000.
34. K. Yang, J. E. Boles, L. J. White, K. L. F. Hilton, H. Y. Lai, Y. Long, J. R. Hiscock and C. J. E. Haynes, *RSC Adv*, 2022, **12**, 27877-27880.
35. D. A. McNaughton, T. Y. T. To, B. A. Hawkins, D. E. Hibbs and P. A. Gale, *Org Biomol Chem*, 2021, **19**, 9624-9628.
36. M. J. Spooner and P. A. Gale, *Chem Comm*, 2015, **51**, 4883-4886.
37. L. A. Jowett, E. N. W. Howe, V. Soto-Cerrato, W. Van Rossom, R. Perez-Tomas and P. A. Gale, *Sci Rep*, 2017, **7**, 9397.
38. D. Singh, D. Rajput and S. Kanvah, *Chem Comm*, 2022, **58**, 2413-2429.
39. Y. H. Lee, N. Park, Y. B. Park, Y. J. Hwang, C. Kang and J. S. Kim, *Chem Comm*, 2014, **50**, 3197-3200.

40. A. Kamkaew, S. Thavornpradit, T. Puangsamlee, D. Xin, N. Wanichacheva and K. Burgess, *Org Biomol Chem*, 2015, **13**, 8271-8276.
41. V. Soto-Cerrato, P. Manuel-Manresa, E. Hernando, S. Calabuig-Farinas, A. Martinez-Romero, V. Fernandez-Duenas, K. Sahlholm, T. Knopfel, M. Garcia-Valverde, A. M. Rodilla, E. Jantus-Lewintre, R. Farras, F. Ciruela, R. Perez-Tomas and R. Quesada, *J Am Chem Soc*, 2015, **137**, 15892-15898.